Journal of Materials Chemistry B

Accepted Manuscript

ROYAL SOCIETY OF CHEMISTRY

www.rsc.org/materialsB

Journal of Materials Chemistry B

Cite this: DOI: 10.1039/c0xx00000x

www.rsc.org/xxxxxx

PAPER

Preparation and antitumor effect evaluation of composite microparticles co-loaded with siRNA and paclitaxel by a supercritical process

Ai-Zheng Chen[*a, b], Yong-Qiang Kang[a], Shi-Bin Wang[a, b], Na Tang[a], Xiao-Qian Su[a]

Received (in XXX, XXX) Xth XXXXXXXXX 200X, Accepted Xth XXXXXXXXX 200X

DOI: 10.1039/b000000x

The co-delivery of siRNA and therapeutic agents provides an effective method for cancer chemotherapy by avoiding drug resistance during the treatment. With a combination of ionic gelation and supercritical fluid technology, nanoparticle-embedded composite microparticles (CMPs) co-loaded with siRNA and paclitaxel (siRNA-PTX-CMPs) were successfully prepared. The results show that CMPs embedded with nanoparticles with a diameter of 50-100 nm exhibited a spherical shape and core-shell structure with a mean diameter of 323 nm. The encapsulation efficiency of siRNA in chitosan nanoparticles (CS NPs) was 96.97%. The drug load and encapsulation efficiency of PTX-loaded CMPs (5% dosage) were 1.40% and 27.95%, respectively; these both increased with an increase in dosage. It was found that no change had occurred in the functional groups of the components during the supercritical process, while the physical form of PTX had shifted to an amorphous state. In the cell experiments, the CMPs clustered around the nucleus after being uptaken by the Bcap-37 cells. The results of the antitumor effect experiments revealed that the co-loaded siRNA-PTX-CMPs achieved a significantly better synergistic effect than single dosages, which indicated that the co-delivery system developed by the supercritical process could have potential in the application of cancer chemotherapy.

Introduction

It is well known that drug resistance, which is the leading cause of cancer-related deaths around the world, is one of the most important challenges encountered in the chemotherapy of cancer.[1-3] According to a previous study,[4] the main mechanisms of drug resistance are grouped into five categories: increased drug efflux, decreased drug influx, DNA repair activation, detoxification, and blockage of apoptosis because of existing drug resistance in the cancer cells. To overcome these barriers, a new and effective method for the fabrication of an appropriate carrier is necessary for the successful delivery of chemotherapy for cancer.[5]

The co-delivery of siRNA and chemotherapy drugs has been shown to have a good synergistic effect in the field of cancer treatment and has attracted a great deal of attention.[6] In a co-delivery system, the siRNA targets the gene of the drug pump, which generally exhibiting a high specificity and low non-specific toxicity thus shutting down the drug pump and facilitating the entry of the chemotherapeutic agent into the cancer cells. Based on the above principle, many studies have proved that the application of gene delivery could effectively reduce the drug resistance.[7, 8] Several different co-delivery systems have been synthesized and these can be grouped into three categories: inorganic-based, lipid-based, and polymer-based.[9] Although inorganic nanoparticles, such as porous silica nanoparticles, have been used as carriers in the treatment of cancer,[10, 11] their toxicity has limited their further application.[10] Many studies have examined the antitumor effect of liposome-based drug carriers co-loaded with siRNA and chemotherapy drugs,[12-15] but there are still some problems, such as inconvenient storage, poor stability, and insufficient protection caused by the drug distribution.[16] The carriers based on polymers such as chitosan and poly (L-lactide)-poly (ethylene glycol)-poly (L-lactide) triblock copolymer (PLLA-PEG-PLLA), which possess the properties of good biocompatibility and low immunogenicity, have also drawn the attention of many researchers and have been widely employed as carriers of genes and drugs in the field of medicine.[17-20] The creation of a safe and effective carrier for application requires not only the appropriate materials but also an effective method.

The conventional methods for producing a drug delivery system, for instance, spray drying and double-emulsion solvent evaporation,[21] have failed in effectively removing the organic solvent to a very low concentration, which has limited their application in the field of medicine.[22] A promising method to prepare carriers for the co-delivery of genes and drugs is an urgent necessity for pharmaceutical applications. Because of its properties of mild operating conditions, very low solvent residue, and low cost, supercritical CO_2 technology has been employed in the study of drug carriers.[23-28] Due to the insolubility of genes in organic solvents, the supercritical process is always combined with emulsion when fabricating carriers loaded with a gene, so that the activity of the gene can be maintained.[29, 30]

In the present study, we attempted to prepare siRNA-PTX-CMPs with the objective of achieving a good therapeutic effect in cancer treatment by the combination of ionic gelation and supercritical technologies, which are environmentally friendly

methods and have been widely used in the fabrication of drug carriers. The CS NPs containing siRNA as core materials were firstly prepared by ionic gelation, and this was followed by encapsulation with PLLA-PEG-PLLA as a shell material by a supercritical process to fabricate the siRNA-PTX-CMPs. The surface morphologies of CS NPs and CMPs were observed; the encapsulation efficiency of siRNA in CS NPs and the profiles of PTX-loaded CMPs were measured; and examinations of cell apoptosis were carried out to evaluate the antitumor effect of siRNA-PTX-CMPs.

Materials and methods

Materials

PLLA-PEG-PLLA (50 kDa) was purchased from the Jinan Daigang Co., Ltd. (Jinan, China). Chitosan and sodium tripolyphosphate were purchased from Aladdin® Co., Ltd. Dulbecco's modified eagle medium (DMEM) and fetal bovine serum were purchased from the American Gibco company. Alamar Blue was purchased from the American Invitrogen Company. Bcap-37 cells (P-gp dependent[31]) were purchased from the Type Culture Collection of the Chinese Academy of Sciences (Shanghai, China). Dichloromethane (DCM, 99.8% purity) was purchased from the Sinopharm Chemical Reagent Co., Ltd. (Shanghai, China). CO_2 of 99.9% purity was supplied by the Rihong Air Products Co., Ltd. (Xiamen, China). All other compounds were of analytical purity.

Methods

Preparation of chitosan nanoparticles loaded with siRNA

The siRNA solution was prepared by adding 2 OD siRNA (for siRNA, 1OD=3.0 nmol=40 ug) to 250 μL of the sodium tripolyphosphate (TPP) solution dissolved in RNase-free water. The siRNA solution was then mixed with 500 μL of the chitosan solution for 1 min under vortex to produce the siRNA-encapsulated CS NPs.

The sequence information of the siRNA targeting the human MRP-1 is as follows:

Sense strand：5'- GUGUCAUCUGAAUGUAGCCTT -3'

Antisense strand：5'- GGCUACAUUCAGAUGACACTT -3'

Preparation of composite microparticles co-loaded with siRNA and PTX

Firstly, the PTX and PLLA-PEG-PLLA were dissolved in the DCM, and the acetone was then added as a non-solvent to the above solution to achieve an oil phase with a high saturation and low concentration. Following this, 1.5 mL of CS NPs with siRNA was added into the oil phase under ultrasonication to obtain a homogeneous solution.

Fig. 1 is a schematic diagram of the process, as described in our previous reports.[32, 33] The apparatus for the fabrication process consists of three major components: a CO_2 supply system, a solution delivery system, and an autoclave with a volume of 500 mL. At the beginning of an experiment, the CO_2 fed from a CO_2 cylinder was cooled down to around 0℃ using a cooler to ensure the liquefaction of the gas and also to prevent cavitation. The liquefied CO_2 was then delivered by a high pressure meter pump through a heat exchanger to preheat the liquefied CO_2 to the desired operating temperature before it entered the autoclave, which was incubated in a gas bath to keep the temperature constant at 35℃ during the experiment. When the desired pressure (12 MPa) was reached, a steady flow of CO_2 (1500 $L \cdot h^{-1}$) was maintained by adjusting the frequency of the CO_2 pump and regulating the downstream valve. The homogeneous solution in the syringe-like cylindrical device was then fed into the autoclave through a nozzle (inner diameter 160 μm) at a flow rate of 2.0 $mL \cdot min^{-1}$. When the spraying of emulsion was finished, a 20 min washing process was performed by continuously pumping fresh CO_2 into the autoclave to remove the residual organic solvent. After washing, the autoclave was slowly depressurized and the powder products, namely the CMPs, were obtained for further characterizations.

Charaterization of morphologies

The samples were absorbed onto the conducting resin and then sprayed with gold under vacuum conditions. Scanning electron microscopy (S-4800 UHR FE-SEM, Hitachi, Japan) was used to investigate the surface morphologies of the samples.

A copper micro-grid supporting a carbon-coated film was used as a sample holder. The aqueous solution of the samples prepared by ultrasonication was deposited onto the sample holder and dried at room temperature. Transmission electron microscopy (TEM, H-7650, Hitachi, Japan) was used to observe the morphology. Before the observation, only the CS NPs were negatively stained, using phosphotungstic acid.

Investigation of siRNA encapsulation efficiency

An siRNA solution of 5 μmol/L was prepared by adding 300 μL of water to the 0.5 OD siRNA. A series of siRNA standard solutions was obtained by mixing 1, 2, 4, 6, 8, and 10 μL of this siRNA solution, respectively, with DEPC water to a fixed volume of 20 μL. Five microliters of the RNA buffer solution was added to the siRNA standard solutions and siRNA-loaded CS NP suspensions, respectively, followed by mixing on a vortex apparatus. Ten microliters of the solution was then added to the lane of agarose gel to conduct electrophoresis under 100 V for 30 min. A photo of the gel electrophoresis was obtained using the gel imaging system. The Image J software was applied to convert the electrophoretic bands to optical density. The standard curve between sample concentration and optical density was then plotted. The encapsulation efficiency of siRNA in CS NPs was calculated according to the standard curve.[34]

Measurements of the drug load and encapsulation efficiency of PTX

For the determination of drug load (DL) and encapsulation efficiency (EE), 10 mg samples of CMPs with different dosages of PTX (2%, 5%, and 10%) were dissolved in DCM; methyl alcohol was then added to dissolve the PTX and precipitate the PLLA-PEG-PLLA. The solution containing PTX was filtered through a 0.22 μm membrane and the concentration of PTX in the solution was analyzed by HPLC. In the HPLC, the chromatographic column was C18 (150 mm×4.6 mm), the mobile phase was methanol and water (70:30, v/v), and the flow rate of the mobile phase was 1.0 mL/min. The DL and EE were calculated according to equation (1) and equation (2) listed below:

$DL = W_1/W_2 \times 100\%$ (1) and

$EE = W_1/W_3 \times 100\%$ (2),

where W_1, W_2, and W_3 represent the total weight of PTX in the CMPs, the weight of the CMPs, and the weight of PTX added within the fabrication process, respectively. Each experiment was done in triplicate.

Characterization of the physicochemical properties of the CMPs

A Fourier transform infrared spectroscope (FTIR) 8400S (SHIMADZU) was employed to estimate the influence of the process on the functional groups of the materials. Before analysis, the samples were gently mixed with KBr and then pressed into a transparent flake. Differential scanning calorimetry (DSC) was used for the evaluation of the thermodynamic properties of the materials before and after the fabrication process, in which the samples were heated from 30℃ to 200℃ at a rate of $10℃ \cdot min^{-1}$.

Study of the antitumor effect of the CMPs

Uptake of the CMPs by cells

The blank CMPs were firstly labeled using rhodamine. When the density of the cells seeded on the confocal special dish was 80%, the culture medium was replaced by the culture suspension containing 0.5 mg/mL of rhodamine-labeled CMPs, and this was incubated at 37℃ for a set time. After discarding the culture medium and washing the cells with PBS, the cells were fixed with 4% paraformaldehyde and then washed with PBS. Next, the cytoskeleton and nucleus of the cells was stained with FITC-phalloidin and Hoechst 33258, respectively. Finally, the laser scanning confocal microscope (LSCM) was used to observe the uptake of CMPs by Bcap-37 cells.

Evaluation of cell apoptosis by AO/EB

The Bcap-37 cells seeded on the 24-well plates were treated with blank CMPs culture suspension, PTX-CMPs culture suspension, and siRNA-PTX-CMPs culture suspension at a concentration of 500 μg/mL, respectively. Cells without treatment were used as a control. At the set point, cells were trypsinized, collected, and resuspended in the PBS buffer in sequence. According to the specification of the AO/EB kit, the 25 μL of the cell suspension was mixed with 1 μL of the mixed reagent and placed in the dark for dyeing. Finally, LSCM was used to observe the stained cells.

Determination of the antitumor effect by Alamar Blue

The Bcap-37 cells seeded on the 96-well plates were treated with 200 μL of blank CMPs culture suspension, PTX-CMPs culture suspension, and siRNA-PTX-CMPs culture suspension at a concentration of 500 μg/mL, respectively. Cells without treatment were used as a control. At the set point, the above culture in the 96-well plates was replaced by 100 μL of fresh cultures with 10% Alamar Blue, and the cells were incubated for 4 h. The absorbance of each well was then measured using a microplate reader under the wavelengths of 570 nm and 600 nm. The relative growth rate (RGR) was defined as the antitumor effect of siRNA-PTX-CMPs. The RGR was calculated according to the following equation:

RGR%=absorbance of sample group (OD_{570}-OD_{600}) / absorbance of control group (OD_{570}-OD_{600}).

Statistical analysis

The mean ± SD was determined for each treatment group. Statistical analysis was performed using a Student's *t*-test. The differences were considered significant for *$p<0.05$ and very significant for **$p<0.01$.

Results and discussion

Morphology and siRNA encapsulation efficiency of the CS NPs

In the ionic gelation, the tripolyphosphoric groups of TPP linked with the ammonium group of chitosan via electrostatic interaction, thus forming the CS NPs,[35] in which the siRNA with a negative charge also linked the positively charged chitosan and was encapsulated in the CS NPs. Fig. 2 shows that the CS NPs containing siRNA exhibited a spherical morphology, and the diameter ranged from 50 nm to 100 nm. Compared with the blank CS NPs, as shown in Fig. 3, the zeta potential of siRNA-loaded CS NPs was lower because the positive charge of CS NPs was neutralized by the negative charge of siRNA. The siRNA encapsulation efficiency was 96.97%, as calculated from Fig. 4, which indicated that the ionic gelation was an effective process by which to encapsulate siRNA into CS NPs as a gene carrier. This result is consistent with the previous studies.[36] Subsequently, the CS NPs were used as the core material to prepare the siRNA-PTX-CMPs, in which the siRNA could successfully be protected by the polymer shell material.

Morphologies and particle size distribution of the CMPs

During the supercritical process, the co-precipitation of PTX and PLLA-PEG-PLLA on the surface of CS naoparticles happened with the expansion and extraction of DCM caused by supercritical carbon dioxide. It can be observed from Fig. 5 that the CMPs exhibited a core-shell structure in which several nanoparticles were encapsulated by the shell. In the image, the inner dark-colored particles are the CS nanoparticles and the outer particles with an irregular morphology are the PLLA-PEG-PLLA shells, thus displaying the core-shell structured, nanoparticle-embedded CMPs. The mean diameter of the CMPs measured by the nano measurer was 320 nm. As illustrated in Fig. 6, the mean diameter of the PTX-CMPs increased slowly from 345 nm to 393 nm with the increase in the dosage of the PTX-CMPs from 2% to 10%; however, this result revealed that the effect of different drug loads on the size of the final CMPs was not significant. This could also be verified by the morphologies of the PTX-CMPs with different drug dosages, which showed no significant differences, as shown in Fig. 7.

Drug load, encapsulation efficiency, and physicochemical properties of the CMPs

Under fixed conditions, the retention time of PTX was between 8 and 9 min. As shown in Fig. 8, the drug loads of PTX-loaded CMPs with dosages of 2%, 5%, and 10% were 0.75%, 1.40%, and 5.40%, respectively, which indicated that there was a great loss of PTX during the supercritical processing because PTX is soluble in supercritical CO_2 to some extent.[37] With the increase in PTX dosages, the percentage of PTX lost in the supercritical CO_2 decreased due to its limited solubility in supercritical CO_2; thus, more PTX was precipitated in the CMPs, with a higher

encapsulation efficiency. However, the encapsulation efficiency did not noticeably change the morphology of the PTX-CMPs. The reason for this could be that the PTX-CMPs were fluffy microparticles and an increase in the precipitated PTX made the particles more dense but not larger.

As shown in the FTIR curves in Fig. 9, the two sharp and intense peaks at 1759 cm^{-1} and 1089 cm^{-1} in CMPs composed of PLLA-PEG-PLLA referred to the carboxylic ester (C=O) and ether (C-O-C) groups, respectively. The characteristic absorption peak at 3490 cm^{-1} represented the hydroxyl group located in the end group of PLLA-PEG-PLLA.[38] Some strong absorption peaks were observed in the FTIR spectrum of raw PTX. The peaks in the regions of 1590-1735 cm^{-1} and 1045-1068 cm^{-1} corresponded to the aromatic ring stretching frequency and the presence of aromatic C-H bonds, respectively. In addition, the peak at 1649 cm^{-1} was due to the C=O amide stretching of PTX and the peak at 1244 cm^{-1} was due to C-O-C stretching. These characteristic peaks in raw PTX are consistent with previous studies.[39, 40] The same phenomenon was apparent in the FTIR curve of the PTX-CMPs. Compared to the FTIR curves of raw PTX and the CMPs, the absorption peaks of the PTX-CMPs were stronger and no new peak existed in the FTIR curve of PTX-loaded CMPs, indicating that the PTX had been encapsulated in the CMPs by a physical process, without any change in the functional groups of the materials used. In this process, the CS NPs containing siRNA as the core material were firstly prepared by ionic gelation, and this was followed by encapsulation in PLLA-PEG-PLLA as a shell material by a supercritical process to fabricate the siRNA-PTX-CMPs. There would not be any interaction between siRNA and PTX since they are in different spaces, and this is also consistent with the results of FTIR and the antitumor effect experiment.

It can be observed from Fig. 10 that the raw PLLA-PEG-PLLA possessed two melting peaks (170.6℃ and 177.4℃), but the melting temperature of the material in the CMPs was 172.4℃, indicating that the crystalline form of PLLA-PEG-PLLA was more homogeneous after the supercritical processing. The DSC curve of raw PTX showed an endothermic dehydration at 82.6℃ because of the water of crystallization in it.[41] The melting process of PTX was not observed in this measurement, since the temperature range here was 20 to 200℃, while the melting temperature of raw PTX has been reported to be at about 222℃.[42, 43] In the PTX-CMPs, there was no endothermic peak at 82.6℃, which indicated that the crystalline form of PTX may have changed to the amorphous form due to the loss of crystal water and the effect of the process, and this is favorable for improving the bioavailability of PTX.[44] There was a peak at 128.2℃ in the PTX-CMPs, which may be the endothermic peak of CS NPs, changed from 73.9℃ to 128.2℃ because of their encapsulation in the PTX-CMPs and the change of heat transfer, where the heat arriving at the CS NPs firstly passes through the coating of PLLA-PEG-PLLA. However, Kang et al.[45] reported that the melting temperature of BSA decreased after encapsulation by poly-lactic acid because the secondary structure had been changed. From the two results above, it may be concluded that the melting temperature of the material was affected by the structure of the particle and by its distribution in the carrier.

Cell uptake of the CMPs

Experiments involving the uptake of microparticles by cells have been conducted in many studies. Kang et al.[46] employed LSCM and TEM to observe indomethacin-loaded PLLA/PLGA microparticles with a diameter of 2.35 μm, prepared in a supercritical process, in the cancer treatment of A549 cells, and found that the microparticles could enter A549 cells. Similarly, the CMPs with a mean diameter of 320 nm could also enter the Bcap-37 cells, as shown in Fig. 11. It was assumed that the CMPs had entered the cells as the microparticles gathered around the nucleus of the cells and did not appear in any of the images, and more CMPs were absorbed around the nucleus in 48 hours, a finding which was similar to that of the above study.[46] This result has provided the foundation for the combination therapy of siRNA and PTX, which is expected to achieve a better antitumor effect than using either siRNA or PTX alone.

Antitumor effect of the drug-loaded CMPs

According to the specification of the AO/EB kit, 1 μL of the mixed reagent contained reagent 1, which could enter the living cells and stain them green, and reagent 2, which entered the dead cells and stained them orange. After mixing with the mixed reagent, the cells treated with siRNA-PTX-CMPs could be divided into four categories: green round, green irregular, orange irregular, and orange round. Correspondingly, in Fig. 12, arrow 1 refers to normal cells, arrow 2 refers to viable apoptotic cells, arrow 3 refers to non-viable apoptotic cells, and arrow 4 refers to dead cells.

From Fig. 12, it can be observed that many dead cells existed in the group of siRNA-PTX-CMPs within 48 hours, demonstrating that the CMPs based on PLLA-PEG-PLLA had entered the cells and achieved a good antitumor effect. Chen et al.[47] used methotrexate-loaded PLLA-PEG-PLLA microparticles in the treatment of MG-63 cells and concluded that the drug-loaded microparticles could induce the apoptosis and death of cells, and this supports the above findings.

As shown in Fig. 13, there was no significant difference in RGR among the cells of the three groups in 1 day because of the small amount of CMPs uptaken by the cells in the limited time. As time went on, the RGR of the cells in the PTX-CMPs group at 3 days and 5 days was 79.9% and 82.6%, respectively, while the RGR of the cells in the blank CMPs group was above 80% at both 3 and 5 days. However, the RGR of the cells in the siRNA-PTX-CMPs at 3 days and 5 days was 67.7% and 59.1%, respectively. This result is consistent with a previous study on in vitro cytotoxicity of PTX against other tumor cells.[48] The reason for this finding could be that for longer incubation periods, the PTX is more active.[49] At the same time, more siRNA encapsulated in CS NPs could be released to perform sufficiently so that a reduction of RGR was detected. After statistical analysis, it was found that a significant difference existed in the antitumor effect between the PTX-CMPs group and the siRNA-PTX-CMPs group, since the Bcap-37 cell used in this study is P-gp dependent strain, which can overexpress P-gp and has a drug-resistance property,[50] this reveals that the siRNA played an important role in synergistic effect with PTX to kill the cancer cells via silencing of P-gp, which thus shutting down the drug pump and facilitating the entry of PTX into the cancer cells. These phenomena indicate that the siRNA-PTX-CMPs had achieved a better synergistic

antitumor effect and would be a promising method in the delivery of cancer chemotherapy.

Conclusions

CMPs with a core-shell structure and a mean diameter of 323 nm, which could be co-loaded with siRNA and PTX for cancer treatment, were successfully fabricated by supercritical fluid technology. The drug loading performance and physicochemical properties of the CMPs have shown that the supercritical process could be employed to produce carriers suitable for the co-delivery of a gene and a chemotherapy drug. Moreover, the results of antitumor effect experiments have demonstrated that the siRNA-PTX-CMPs obtained a much better antitumor effect than the CMPs encapsulated with PTX alone. In conclusion, this study reveals that the gene and drug co-delivery system developed by the supercritical process has potential in the application of cancer chemotherapy without drug resistance.

Acknowledgements

Financial supports from Natural Science Foundation of China (31470927 and 31170939), Natural Science Foundation of Fujian Province of China (2014J01128), Public Science and Technology Research Funds Projects of Ocean (201505029) and Promotion Program for Young and Middle-aged Teacher in Science and Technology Research of Huaqiao University (ZQN-PY107) are gratefully acknowledged.

Notes and references

[a] *College of Chemical Engineering, Huaqiao University, Xiamen, China. Fax: +86-592-6162326; Tel: +86-592-6162326;*
[b] *Institute of Biomaterials and Tissue Engineering, Huaqiao University, Xiamen, China;*
* *E-mail: azchen@hqu.edu.cn; Tel: +86-592-6162326; Fax: +86-592-6162326;*

1. M. M. Gottesman, *Annu. Rev. Med.*, 2002, **53**, 615-627.
2. N. Jonckheere, N. Skrypek and I. Van Seuningen, *BBA-Rev. Cancer*, 2014, **1846**, 142-151.
3. W. J. Li, J. Shi, C. Zhang, M. Li, L. Gan, H. B. Xu and X. L. Yang, *J. Mat. Chem. B*, 2014, **2**, 4901-4910.
4. M. M. Gottesman, T. Fojo and S. E. Bates, *Nat. Rev. Cancer*, 2002, **2**, 48-58.
5. C. M. J. Hu and L. F. Zhang, *Biochem. Pharmacol.*, 2012, **83**, 1104-1111.
6. V. Tsouris, M. K. Joo, S. H. Kim, I. C. Kwon and Y. Y. Won, *Biotechnol. Adv.*, 2014, **32**, 1037-1050.
7. A. Mitha and M. Rekha, *J. Mat. Chem. B*, 2014, **2**, 8005-8016.
8. M. Wu, Y. Chen, L. Zhang, X. Li, X. Cai, Y. Du, L. Zhang and J. Shi, *J. Mat. Chem. B*, 2015, **3**, 766-775.
9. M. Creixell and N. A. Peppas, *Nano Today*, 2012, **7**, 367-379.
10. H. C. Huang, S. Barua, G. Sharma, S. K. Dey and K. Rege, *J. Control. Release*, 2011, **155**, 344-357.
11. M. J. Sailor and J. H. Park, *Adv. Mater.*, 2012, **24**, 3779-3802.
12. W. S. Lin, Y. W. Huang, X. D. Zhou and Y. F. Ma, *Toxicol. Appl. Pharmacol.*, 2006, **217**, 252-259.
13. M. H. Qu, R. F. Zeng, S. Fang, Q. S. Dai, H. P. Li and J. T. Long, *Int. J. Pharm.*, 2014, **474**, 112-122.
14. M. Saad, O. B. Garbuzenko and T. Minko, *Nanomed.*, 2008, **3**, 761-776.
15. S. H. Kang, H. J. Cho, G. Shim, S. Lee, S. H. Kim, H. G. Choi, C. W. Kim and Y. K. Oh, *Pharm. Res.*, 2011, **28**, 3069-3078.
16. Y. Y. Zhang and J. M. Chen, *Acta Pharm. Sinica*, 2011, **46**, 261-268.
17. T. A. Sonia and C. P. Sharma, *Chitosan for Biomaterials I*, 2011, **243**, 23-53.
18. G. Ruan and S. S. Feng, *Biomaterials*, 2003, **24**, 5037-5044.
19. C. Perez, A. Sanchez, D. Putnam, D. Ting, R. Langer and M. J. Alonso, *J. Control. Release*, 2001, **75**, 211-224.
20. W. W. Zou, C. X. Liu, Z. J. Chen and N. Zhang, *Nanoscale Res. Lett.*, 2009, **4**, 982-992.
21. F. T. Meng, G. H. Ma, Y. D. Liu, W. Qiu and Z. G. Su, *Colloid. Surface. B.*, 2004, **33**, 177-183.
22. J. Qu, Y. Liu, Y. Yu, J. Li, J. Luo and M. Li, *Mat. Sci. Eng. C-Mater.*, 2014, **44**, 166-174.
23. O. R. Davies, A. L. Lewis, M. J. Whitaker, H. Y. Tai, K. M. Shakesheff and S. M. Howdle, *Adv. Drug Deliver. Rev.*, 2008, **60**, 373-387.
24. U. B. Kompella and K. Koushik, *Crit. Rev. Ther. Drug Carrier Syst.*, 2001, **18**, 173-199.
25. M. J. Cocero, A. Martin, F. Mattea and S. Varona, *J. Supercrit. Fluid.*, 2009, **47**, 546-555.
26. A. Z. Chen, L. Li, S. B. Wang, C. Zhao, Y. G. Liu, G. Y. Wang and Z. Zhao, *J. Supercrit. Fluid.*, 2012, **67**, 7-13.
27. A. Z. Chen, Y. Li, F. T. Chau, T. Y. Lau, J. Y. Hu, Z. Zhao and D. K. W. Mok, *Acta Biomater.*, 2009, **5**, 2913-2919.
28. A. Z. Chen, C. Zhao, S. B. Wang, Y. G. Liu and D. L. Lin, *J. Mat. Chem. B*, 2013, **1**, 2967-2975.
29. G. B. Jacobson, E. Gonzalez-Gonzalez, R. Spitler, R. Shinde, D. Leake, R. L. Kaspar, C. H. Contag and R. N. Zare, *J. Pharm. Sci.*, 2010, **99**, 4261-4266.
30. J. Ge, G. B. Jacobson, T. Lobovkina, K. Holmberg and R. N. Zare, *Chem. Commun.*, 2010, **46**, 9034-9036.
31. R. Zhang, S. B. Wang, A. Z. Chen, W. G. Chen, Y. G. Liu, W. G. Wu, Y. Q. Kang and S. F. Ye, *J. Biomater. Appl.*, 2015, 0885328215579297.
32. A. Z. Chen, G. Y. Wang, S. B. Wang, L. Li, Y. G. Liu and C. Zhao, *Int. J. Nanomed.*, 2012, **7**, 3013-3022.
33. A. Z. Chen, Y. Li, D. Chen and J. Y. Hu, *J. Mater. Sci.: Mater. Med.*, 2009, **20**, 751-758.
34. Y. Shen, J. S. Tu, H. Pang and J. B. Zhu, *Acta Pharm. Sinica*, 2009, **44**, 430-435.
35. Y. Xu and Y. Du, *Int. J. Pharm.*, 2003, **250**, 215-226.
36. H. Katas and H. O. Alpar, *J. Control. Release*, 2006, **115**, 216-225.
37. N. Luo, Y. Lu and Y. Jiang, *Chinese J. Chem. Eng.*, 2011, **19**, 558-564.
38. S. P. Zhan, L. Y. Cui, Q. C. Zhao, J. C. Wang, S. H. Chen and S. Q. Ding, *Particul. Sci. Technol*, 2014, **32**, 61-69.
39. G. D. Venkatasubbu, S. Ramasamy, G. Avadhani, V. Ramakrishnan and J. Kumar, *Powder Technol.*, 2013, **235**, 437-442.
40. E. Bilensoy, O. Gürkaynak, M. Ertan, M. Şen and A. A. Hıncal, *J. Pharm. Sci.*, 2008, **97**, 1519-1529.
41. R. T. Liggins, W. L. Hunter and H. M. Burt, *J. Pharm. Sci.*, 1997, **86**, 1458-1463.
42. J. W. Xie and C. H. Wang, *Pharm. Res.*, 2006, **23**, 1817-1826.
43. C. Zhang, Q. N. Ping and H. J. Zhang, *Colloid. Surface. B.*, 2004, **39**, 69-75.
44. Y. Q. Kang, J. Wu, G. F. Yin, Z. B. Huang, X. M. Liao, Y. D. Yao, P. Ouyang, H. J. Wang and Q. Yang, *Langmuir*, 2008, **24**, 7432-7441.
45. Y. Q. Kang, C. Yang, O. Y. Ping, G. F. Yin, Z. B. Huang, Y. D. Yao and X. M. Liao, *Carbohyd. Polym.*, 2009, **77**, 244-249.
46. Y. Q. Kang, J. Wu, G. F. Yin, Z. B. Huang, Y. D. Yao, X. M. Liao, A. Z. Chen, X. M. Pu and L. Liao, *Eur. J. Pharm. Biopharm.*, 2008, **70**, 85-97.
47. A. Z. Chen, T. T. Dang, S. B. Wang, N. Tang, Y. G. Liu and W. G. Wu, *Sci. China Life Sci.*, 2014, **57**, 698-709.
48. C. Fonseca, S. Simões and R. Gaspar, *J. Control. Release*, 2002, **83**, 273-286.
49. N. Lopes, E. Adams, T. Pitts and B. Bhuyan, *Cancer Chemoth. Pharm.*, 1993, **32**, 235-242.
50. Y. Wang, J. Cao and S. Zeng, *World J Gastroenterol.*, 2004, **10**, 1365-1368.

Journal of Materials Chemistry B

Cite this: DOI: 10.1039/c0xx00000x

www.rsc.org/xxxxxx

PAPER

Figure captions

Fig. 1 Schematic diagram for preparation of the siRNA-PTX-CMPs.
Fig. 2 TEM image of the siRNA-CS NPs.
Fig. 3 Mean diameters and zeta potentials of the CS NPs before and after loading with siRNA.
Fig. 4 Photographs of siRNA electrophoresis (a: standard curve of siRNA; b:optical density of each lane; c: photograph of siRNA-CS NPs).
Fig. 5 TEM images of the CMPs under optimal conditions (a: original image; b: with a scale mark).
Fig. 6 Mean diameters of the PTX-CMPs with different drug dosages.
Fig. 7 SEM images of the PTX-CMPs with different drug dosages.
Fig. 8 Drug load and encapsulation efficiency of the PTX-CMPs.
Fig. 9 FTIR spectra of the raw PTX, CMPs, and PTX-CMPs.
Fig. 10 DSC curves of the raw PTX, CS NPs, and PTX-CMPs.
Fig. 11 Intracellular location of the CMPs in Bcap-37 cells (the CMPs are red; the nuclei are blue; and the cytoskeletons are green).
Fig. 12 Antitumor activity of drug-loaded CMPs detected by AO/EB (100×).
Fig. 13 In vitro antitumor effect of the drug-loaded CMPs (When appropriate, statistical significance is indicated: "*": $p<0.05$).

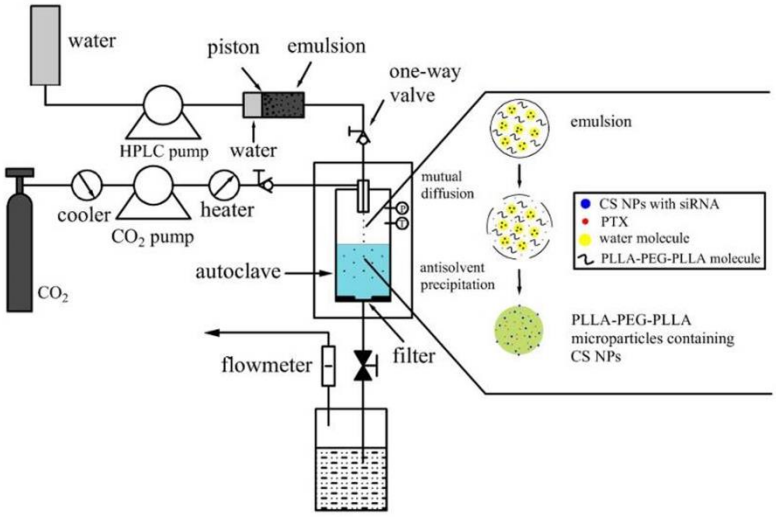

Fig. 1 Schematic diagram for preparation of the siRNA-PTX-CMPs

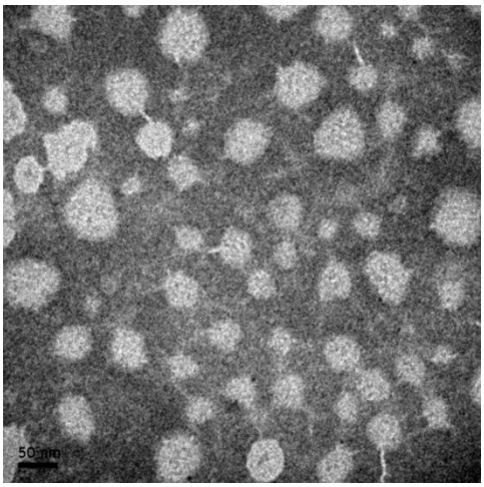

Fig. 2 TEM image of the siRNA-CS NPs

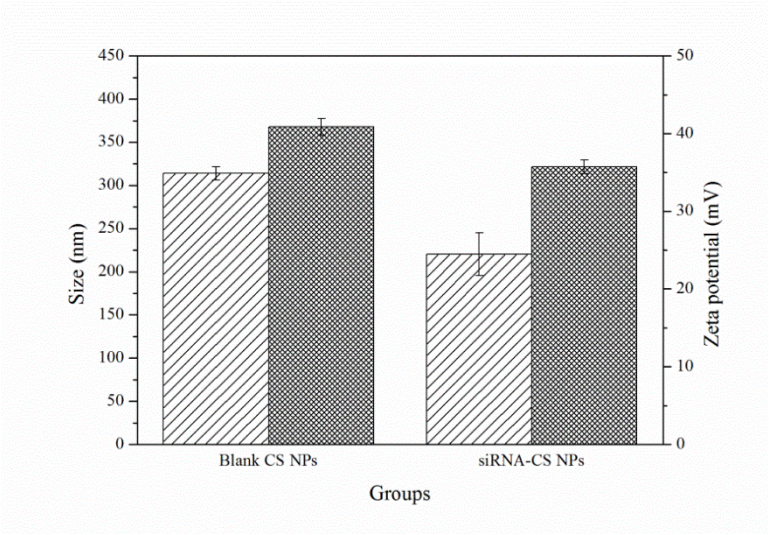

Fig. 3 Mean diameters and zeta potentials of the CS NPs before and after loading with siRNA

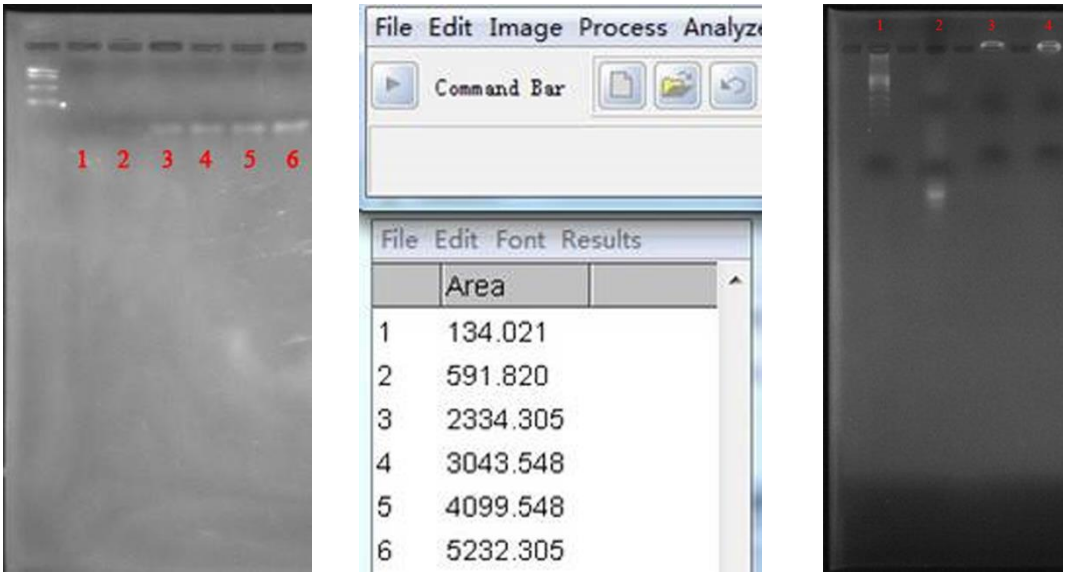

(a) (b) (c)

Fig. 4 Photographs of siRNA electrophoresis (a: standard curve of siRNA; b:optical density of each lane; c: photograph of siRNA-CS NPs)

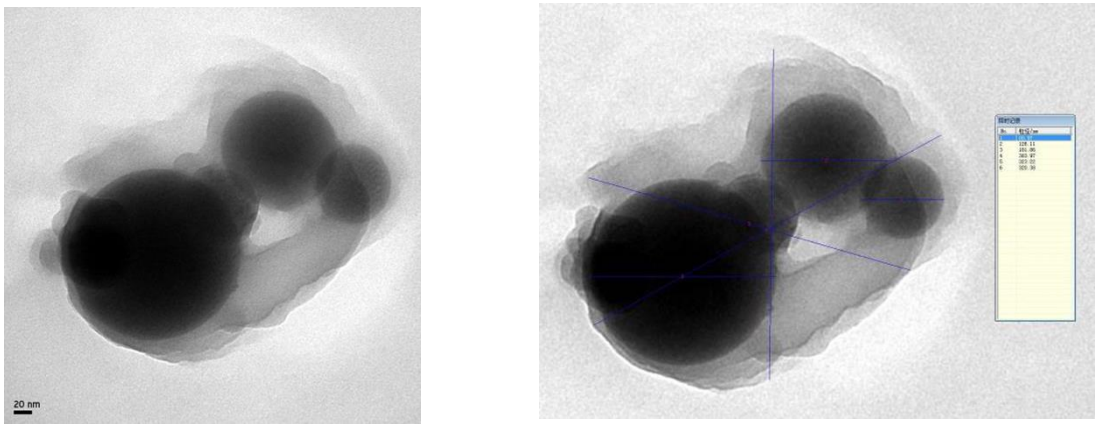

(a) (b)

Fig. 5 TEM images of the CMPs under optimal conditions (a: original image; b: with a scale mark)

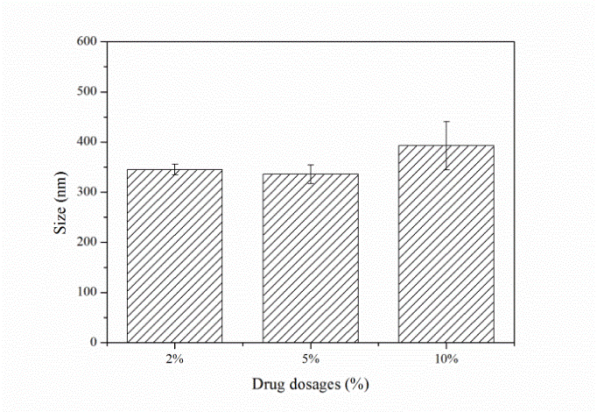

Fig. 6 Mean diameters of the PTX-CMPs with different drug dosages

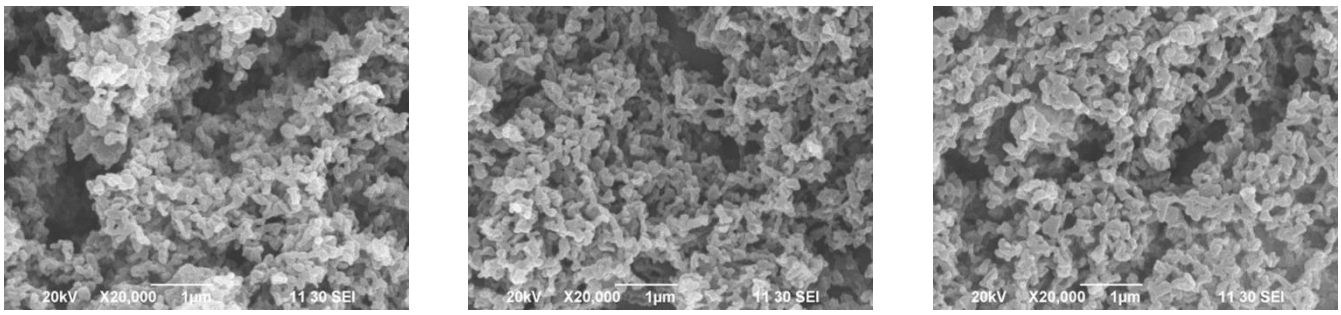

(a) 2% (b) 5% (c) 10%

Fig. 7 SEM images of the PTX-CMPs with different drug dosages

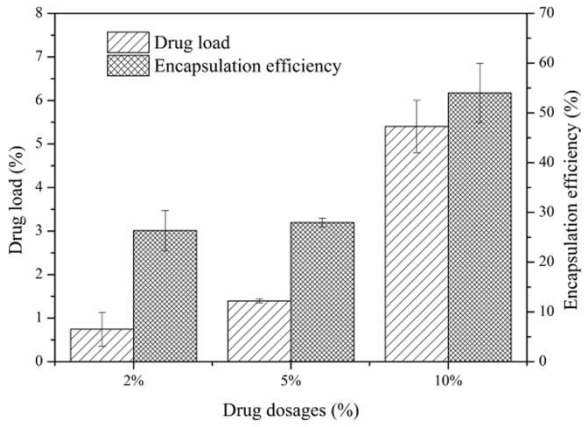

Fig. 8 Drug load and encapsulation efficiency of the PTX-CMPs

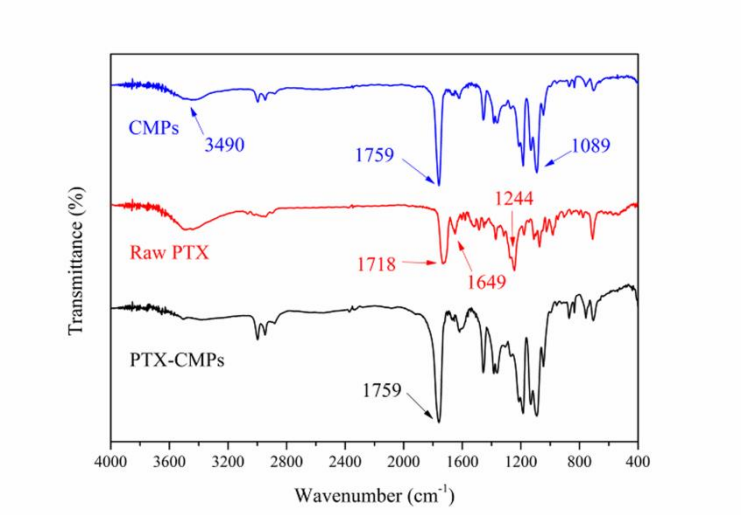

Fig. 9 FTIR spectra of the raw PTX, CMPs, and PTX-CMPs

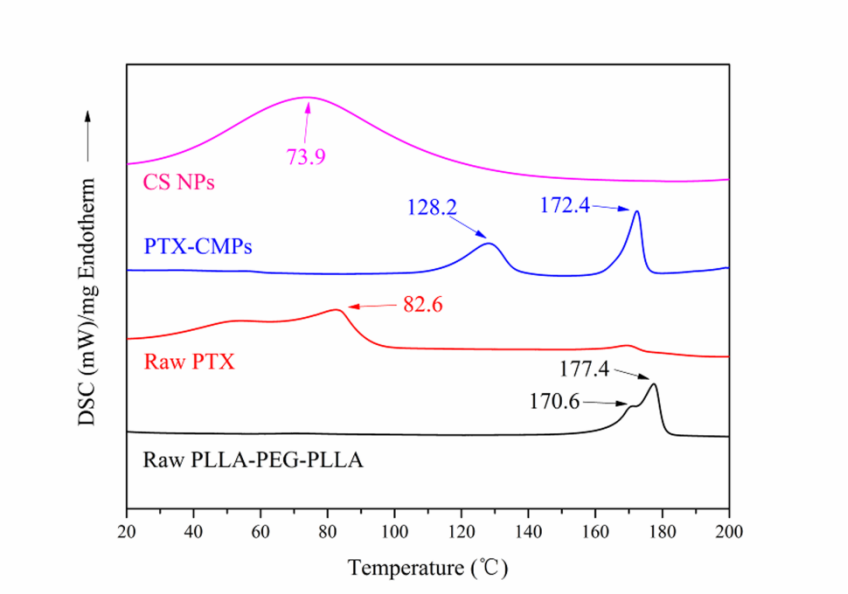

Fig. 10 DSC curves of the raw PTX, CS NPs, and PTX-CMPs

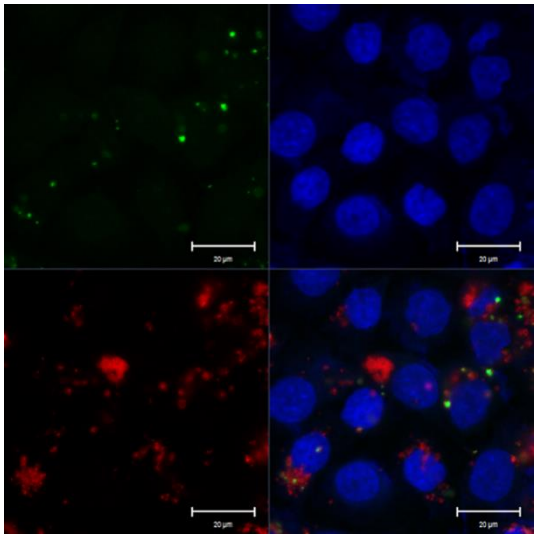

Fig. 11 Intracellular location of the CMPs in Bcap-37 cells (the CMPs are red; the nuclei are blue; and the cytoskeletons are green)

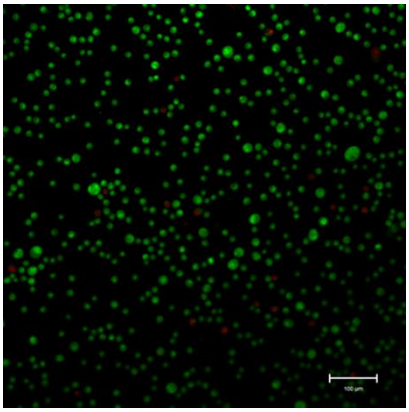

（a）negative control

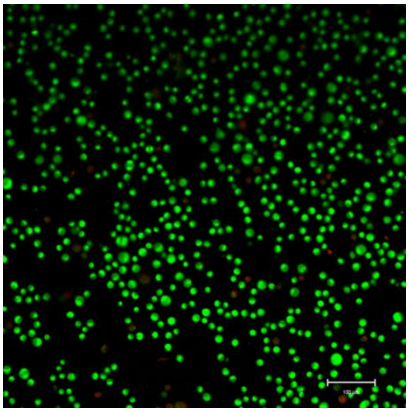

（b）blank CMPs

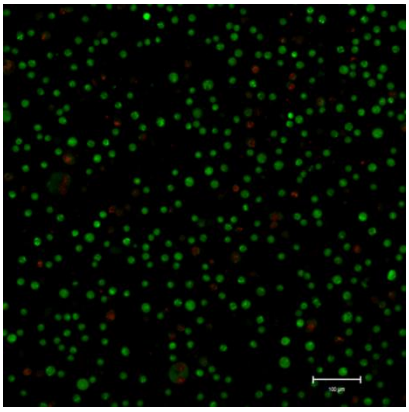

（c）PTX-CMPs

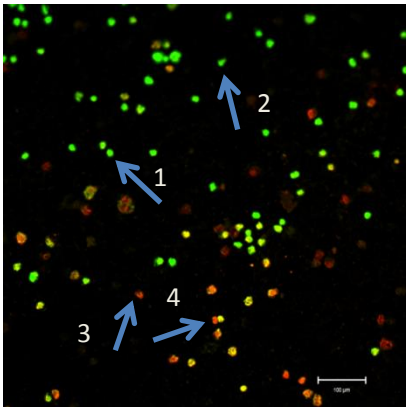

（d）siRNA-PTX-CMPs

Fig. 12 Antitumor activity of drug-loaded CMPs detected by AO/EB (100×)

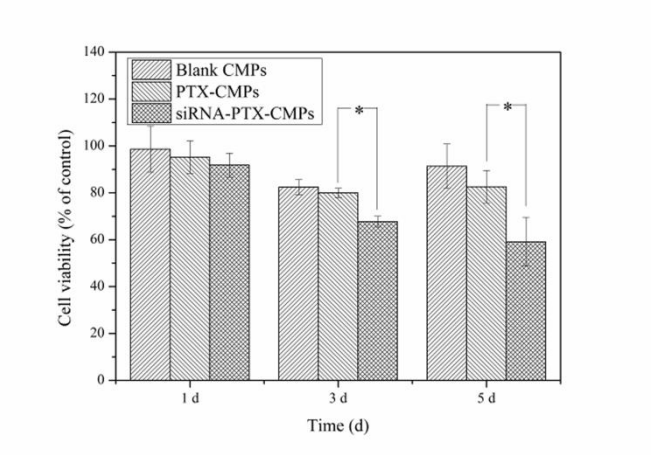

Fig. 13 In vitro antitumor effect of the drug-loaded CMPs (When appropriate, statistical significance is indicated: "*": $p<0.05$)

Table of contents entry

Nanoparticle-embedded composite microparticles co-loaded with siRNA and paclitaxel achieve a significantly better synergistic effect than single dosage.